Supporting information for:

Crystal engineering of a new platform of hybrid ultramicroporous materials and their C_2H_2/CO_2 separation properties

Daniel J. O'Hearn,†[a] Debobroto Sensharma,†[a] Asif Raza,†[a] Andrey A. Bezrukov,[a] Matthias Vandichel,[a*] Soumya Mukherjee,[a,b*] and Michael J. Zaworotko[a,b*]

[a]*Department of Chemical Sciences, Bernal Institute, University of Limerick, Limerick V94 T9PX, Ireland.*
[b]*SSPC, Science Foundation Ireland Research Centre for Pharmaceuticals, University of Limerick, Limerick V94 T9PX, Ireland.*
† These authors contributed equally to this work
* Correspondence address: matthias.vandichel@ul.ie (M.V.) soumya.mukherjee@ul.ie (S.M.) xtal@ul.ie (M.J.Z.)

Contents

1. Synthesis:

1.1. Materials and Methods:

All reactions were performed in air. All reagents/reactants were used as received without further purification and purchased from Tokyo Chemical Industry (4-pyridinecarboxaldeyde, ethylenediamine, sodium borohydride), or Sigma Aldrich/Millipore (zinc hexafluorosilicate hydrate, zinc sulfate heptahydrate), and methanol was purchased from Lennox, and used as received. N^1,N^2-bis(pyridin-4-ylmethyl)ethane-1,2-diamine (**enmepy**) was prepared following a previously reported procedure. [1]

1.2. Bulk synthesis of SOFOUR-2-Zn

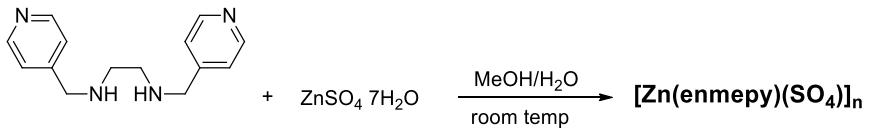

$ZnSO_4 \cdot 7H_2O$ (115 mg, 0.4 mmol) was stirred in deionised water. Once fully dissolved, a MeOH solution of **enmepy** (96 mg, 0.4 mmol, 5 mL MeOH) was added, resulting in a white suspension. This was stirred overnight at room temperature, then filtered using a 0.4 μm membrane filter, washed with MeOH, and dried in air. Yield: 151 mg 75% (assuming 20% weight loss inferred from TGA)

1.3. Bulk synthesis of SIFSIX-24-Zn

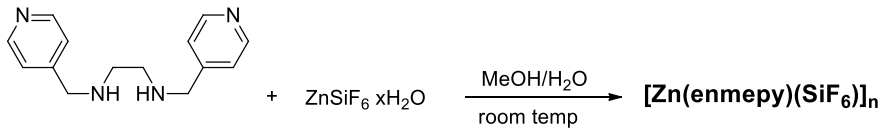

$ZnSiF_6 \cdot xH_2O$ (126 mg, 0.4 mmol (assuming hexahydrate)) was stirred in deionised water. Once fully dissolved, a MeOH solution of **enmepy** (96 mg, 0.4 mmol, 5 mL MeOH) was added, resulting in a white precipitate. This was stirred overnight at room temperature, then filtered using a 0.4 μm membrane filter, washed with MeOH, and dried in air. Yield: 153 mg, 68% (assuming 20% weight loss inferred from TGA).

1.4. Single crystals of SIFSIX-24-Zn

In an NMR tube, 400 μL of a MeOH **enmepy** solution (0.03 mmol/mL) was layered over 400 μL of an ethylene glycol solution of $ZnSiF_6$ (0.03 mmol/mL). 200 μL of a 1:1 mixture of MeOH/ethylene glycol was used as a buffer layer. After 2-3 weeks, crystals suitable for SCXRD were obtained.

2. Characterisation:

2.1. Single Crystal X-ray Diffraction:

A suitable crystal of **SIFSIX-24-Zn** were chosen for single crystal X-ray diffraction measurements. The data was collected at 100 K on a Bruker D8 Quest diffractometer equipped with a CuKα microfocus source (λ = 1.5406 Å) and a Photon 100 detector. Diffraction images were collected in shutterless mode, and were indexed, integrated and scaled in APEX4. [2] Absorption correction was performed by the multi-scan method using SADABS.[3] Space group determination was performed simultaneously with structure solution using SHELXT intrinsic phasing and the solution was refined on F^2 using SHELXL non-linear least squares implemented in Olex^2 v1.2.10.[4-6] All non-hydrogen atoms were refined anisotropically, and hydrogen atoms bonded to carbon were added at calculated positions and refined using the riding model. The hydrogen atom on the coordinating amine group (N2) could not be located and was added to a calculated position using HFIX 13 and refined. The resulting AFIX command was removed, and the hydrogen atom restrained using DFIX to N2 and DANG to the nearest neighbouring hydrogen atoms. The pyridyl ring was constrained as a hexagon using AFIX and its ADPs restrained using RIGU. The bond angle between the methylene carbon C2 and the pyridyl ring was restrained using SADI with s = 0.04. DFIX was also applied between C2 and N2. Residual electron density found in the void space of the structure was treated using the PLATON SQUEEZE routine.[7]

2.2. Powder X-Ray Diffraction (PXRD)

Diffractograms of powder samples were recorded using a PANalytical Empyrean™ diffractometer equipped with a PIXcel3D detector operating in scanning line detector mode with an active length of 4 utilizing 255 channels, in the Continuous Scanning mode with the goniometer in the theta-theta orientation. The diffractometer is fitted with an Empyrean Cu LFF (long fine-focus) HR (9430 033 7310x) tube operated at 40 kV and 40 mA, and CuKα radiation (λ_α = 1.540598 Å) was used for diffraction experiments. Incident beam optics included the Fixed Divergences slit with anti-scatter slit PreFIX module, with a 1/8° divergence slit and a 1/4° anti-scatter slit, as well as a 10 mm fixed incident beam mask and a Soller slit (0.04 rad). Divergent beam optics included a P7.5 anti-scatter slit, a Soller slit (0.04 rad), and a Ni-β filter. The data was collected from 2°-40° (2θ) using a continues scan with a scan rate of 11.8 or 17.2 s/°.

2.3. Thermal gravimetric analysis (TGA)

A TA Q50 thermal gravimetric analyser was used with a 10 K/min ramp rate from ca. 298 K to 823 K under a N_2 flow of 60 mL/min.

3. CSD Search:

The Cambridge Structural database (CSD version 5.45, November 2023 with updates included until September 2024) was searched for structures containing ethylene diamine chelates pillared (bridged to form coordination polymers) by MF_6 and SO_4 (Fig. S1).[8] The search for MF_6 pillared diamine ethylene diamine chelates (described in the Fig. S1a) afforded five hits. Manual inspection resulted in three hits, each of which was an ethylene diamine chelate pillared by MF_6. Further, there are only two distinct compounds in this group that are isostructural. The search for SO_4 pillared diamine ethylene diamine (and its derivatives, and its aromatic equivalent 2-aminoaniline) chelates (described by Fig. S1b) yielded 112 hits. Manual inspection resulted in 25 hits that were chelates pillared by SO_4. Considering the repeat entries presenting the same structure, a total of 20 distinct compounds were found (Table S2; corresponding to chelating ligands listed in Fig. S2). These REFCODEs with their respective chemical formulae and literature references are listed in Tables S1 (MF_6^{2-}) and S2 (SO_4^{2-}). M stands for either of Si, Ge, Sn, and elements belonging to the Group 4 (Ti, Zr and Hf).

4. Single-component gas adsorption:

Materials and Methods:

High-purity gases were used as received from BOC Gases Ireland: He (99.999%), CO_2 (99.995%), C_2H_2 (98.5%). 77 K isotherms were measured using a Micromeritics Tristar II 3030 and bath temperature was maintained by submerging the sample cells in a Dewar filled with liquid N_2. A Micromeritics 3Flex surface area and pore size analyser 3500 was used for collecting the 195, 273 and 298 K isotherms for CO2 and C_2H_2. The temperature at 195 K was maintained by submerging the sample cells in a 4 L Dewar filled with a dry ice-acetone mixture. P_0 for 195 K CO_2 isotherms was considered as 1 bar. Bath temperatures of 273 and 298 K were precisely controlled with a Julabo ME (v.2) recirculating control system containing a mixture of ethylene glycol and water. Prior to experiments, all samples were activated on a SmartVacPrep™ using dynamic vacuum and heating for 24 h at 333 K.

5. Isosteric heat of adsorption (Q_{st}):

Isosteric heats of adsorption (Q_{st}) values were determined using the adsorption branches of isotherms of each adsorbate at 273 K and 298 K. A Virial equation of state (Eqn. 1) was used to fit the isotherm data of C_2H_2 and CO_2 on **SOFOUR-2-Zn** and **SIFSIX-24-Zn**, and combinations of temperatures were used to maximise fit quality to ensure accuracy of the output. [42] P stands for the pressure in Pa, *N* is the adsorbed amount in mmol g^{-1}, T is the temperature in K, a_i and b_i are virial coefficients, and *m* and *n* are the number of coefficients used to describe the isotherms. Q_{st} is the coverage-dependent enthalpy of adsorption and R is the universal gas constant.

$$\ln P = \ln N + \sum_{i=0}^{m} a_i N_i + \sum_{i=0}^{n} \binom{n}{k} b_i N_i \qquad (1)$$

Q_{st} was calculated from the virial model using Eqn. 2.

$$-Q_{st} = -R \sum_{i=0}^{m} a_i N_i \qquad (2)$$

The virial parameters were optimised using non-linear least squares and the resulting fits and optimised parameters are shown in Fig. S12.

6. Water vapour sorption

Dynamic water vapour sorption isotherms were collected using ca. 10 mg each of **SIFSIX-24-Zn** and **SOFOUR-2-Zn** using a DVS Adventure system from Surface Measurement Systems. Temperature was maintained at 300 K by enclosing the system in a temperature-controlled incubator. The mass of the sample was determined in parallel by comparison to an empty reference chamber and recorded by a high-resolution microbalance Ultrabalance Low Mass with a precision of 0.01 μg. Isotherms were measured from 0 to 95% R.H. with an equilibrium criterion dm/dt = 0.05 %/min. The minimum and maximum equilibration times for each step were 10 and 360 min. Before isotherms were collected, samples were activated *in situ* by heating at 333 K for 90 minutes using the built in sample pre-heater. Dry air was used as a carrier gas with a total flow rate of 400 mL min^{-1} (200 mL min^{-1} for each sample).

7. Ideal adsorbed solution theory (IAST) calculations

The selectivity for the adsorbate mixture composition of interest were calculated from the single-component adsorption isotherms using Ideal Adsorbed Solution Theory (IAST).[46, 47] Single-component adsorption isotherms for each gas at 298 K were fit to the thermodynamically consistent single-site Langmuir (Eqn. 3), or dual-site Langmuir equations (Eqn. 4) using pyIAST Python package (Fig. S14).[47]

$$n_i^{\circ}(P) = M\frac{KP}{1+KP} \quad (3)$$

$$n_i^{\circ}(P) = M_1\frac{K_1P}{1+K_1P} + M_2\frac{K_2P}{1+K_2P} \quad (4)$$

Here n_i°, is loading in mmol g^{-1} as a function of pressure (P, bar), M_1 and M_2 are saturation uptakes for sites 1 and 2, respectively in mmol g^{-1}, and K_1 and K_2 are the respective affinity coefficients in units of bar^{-1}. The isotherm parameters were then used to calculate the mole fraction of C_2H_2 and CO_2 in the adsorbed phase (x_i and x_j, respectively) and gas phase (y_i and y_j, respectively) at various pressures. Finally, the selectivity, $S_{i/j}$ at each pressure was calculated using Eqn. 5.

$$S_{i/j} = \frac{(x_i/x_j)}{(y_i/y_j)} \quad (5)$$

These mixture separations are expected to be performed in fixed bed adsorbers, where the process is governed by a combination of adsorption selectivity and capacity. Based on the shock wave model for fixed bed adsorbers, a relevant metric for evaluating separation performance is the separation potential., Δq_I (Eqn. 6).[48,49]

$$\Delta q = q_1\frac{x_1}{x_2} - q_2 \quad (6)$$

For equimolar mixture, $\frac{x_1}{x_2} = 0.5/0.5 = 1$ (see Fig. S15).

8. Dynamic column breakthrough experiments:

8.1. Method

In dynamic column breakthrough (DCB) experiments, 500 -600 mg of pre-activated solid adsorbent was packed in a ¼" (6.35 mm) stainless steel column to form a fixed bed in a Micromeritics Selective Sorption Analyser (SAA). Outlet compositions were monitored using an MKS Cirrus 3 mass spectrometer. Prior to the adsorption branch, the bed was purged with a 20 cm^3 min^{-1} flow of pure He for 3 hours at 333 K and cooled to RT while maintaining He flow. Then, the flow was switched to the desired C_2H_2/CO_2 mixture with the temperature maintained at 298 K for the adsorption branch of the experiment. Once saturation was achieved, the flow was switched to He at 20 cm^3 min^{-1}, and a temperature ramp rate of 5 K per minute was applied until a column temperature of 333 K was achieved. Temperature and He flow were maintained until C_2H_2 and CO_2 outlet concentrations were negligible. Humid C_2H_2/CO_2 experiments were carried out by saturating the CO_2 component of the gas stream with moisture using a bubbler before mixing. Due to instrumental constraints, a high flow rate of 10 cm^3 min^{-1} of CO_2 was required to achieve a stable flow of moisture saturated CO_2 and an additional 5 cm^3 min^{-1} of C_2H_2 was combined with this stream using a mixing valve before entering the sorbent bed. Identical experiments were carried out without moisture to show the effect of moisture on separation.

8.2. Uptakes and Separation Factors

Uptakes were determined from the adsorption branch of the experiments, assuming negligible pressure drop and following Eqn. 6. Dead volume correction was applied by adjusting t_0 to account for time lag between inlet and outlet flows using blank experiments for each inlet mixture composition.

$$q_i = \frac{V_i t_0 - \int_0^{t_0} V_e \, dt}{m} \qquad (7)$$

Here, V_i is the inlet flow rate of gas (cm^3 min^{-1}), V_e is the effluent flow rate of gas (cm^3 min^{-1}), t_0 is the adsorption saturation time (min) and m is the mass of the sorbent (g). The separation factor, α_{AC}, for the DCB experiment is determined using Eqn. 7, where y_i is the partial pressure of gas i in the gas mixture.[50, 51]

$$\alpha = \frac{q_1 y_2}{q_2 y_1} \qquad (8)$$

8.3. Temperature Programmed Desorption (TPD)

Effluent purities in TPD experiments were determined using C_2H_2/CO_2 C/C_0 ratios as normalised using saturation outlet signal values. Productivities of C_2H_2 above the threshold concentration (98% or 99.5%) were determined using Eqn. 9.

$$p_i = \frac{\int_{t1}^{t2} V_e \, dt}{m} \quad (9)$$

Where t_1 and t_2 correspond to the start and end times of the period in which the threshold concentration is surpassed, and other terms are as in Eqn. 7.

9. Molecular Modelling:

Periodic Density Functional Theory (DFT) calculations were performed using the projected augmented wave (PAW) formalism[52] as implemented in the Vienna Ab Initio Simulation Package (VASP 5.4.4),[53,54] employing the BEEF-vdW exchange-correlation functional.[55] Atomic positions and cell parameters were optimised, using the conjugate gradient algorithm with force and electronic convergence criteria of 0.01 eV/Å and 10^{-6} eV, a Gaussian smearing of 0.02 eV, an energy cut-off of 550 eV, and a 2x2x2 Monkhorst-Pack k-point mesh.[56] Plausible adsorption positions of CO_2 and C_2H_2 were optimised in a 1x1x1 unit cell for **SIFSIX-24-Zn** and a 1x1x2 supercell for **SOFOUR-2-Zn**. To verify the binding sites as local minima on the potential energy surface, a partial Hessian vibrational analysis was performed numerically displacing the atomic coordinates of the investigated adsorbates CO_2 and C_2H_2 in x, y, and z-directions with ±0.01 Å. Furthermore, the adsorption enthalpies and zero-point corrected adsorption energies and adsorption Gibbs free energies were calculated with the post-processing toolkit TAMKIN at a temperature of 298 K and adsorbate pressures of 1 bar.[57]

10. Supplementary Figures:

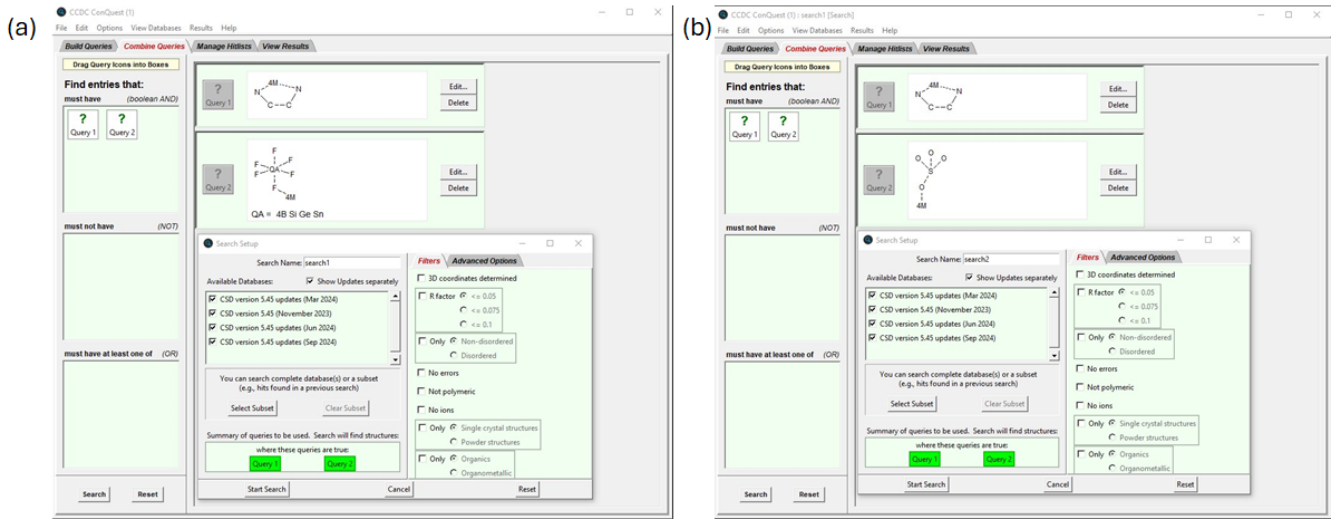

Fig. S1: ConQuest queries used to search the CSD database for ethylene diamine chelates pillared by (a) MF_6 and (b) SO_4. C-N bonds were specified as "single", and all other bonds were specified as "*any*". M stands for either of Si, Ge, Sn, and elements belonging to the Group 4 (Ti, Zr and Hf).

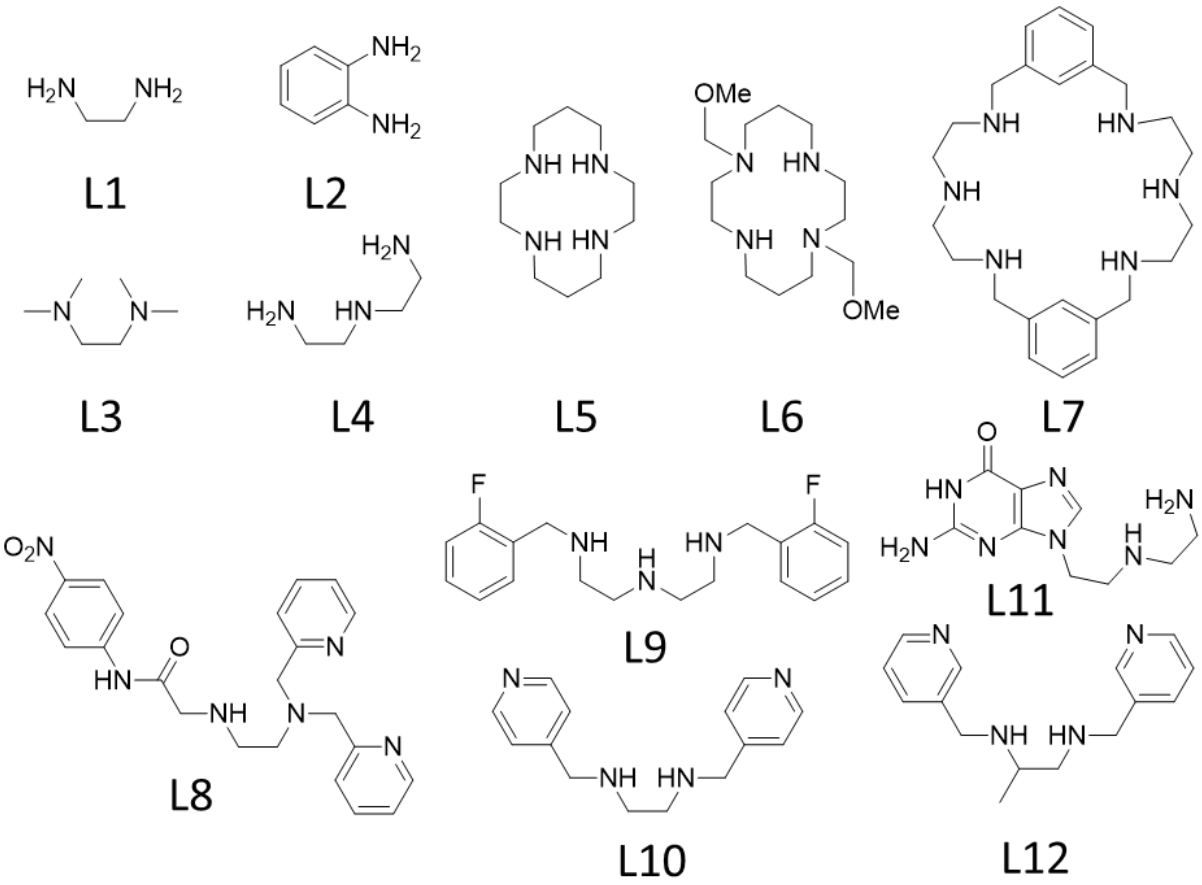

Fig. S2: Chemical structures and corresponding numbers for all the chelating ligands found in our in-house CSD search.

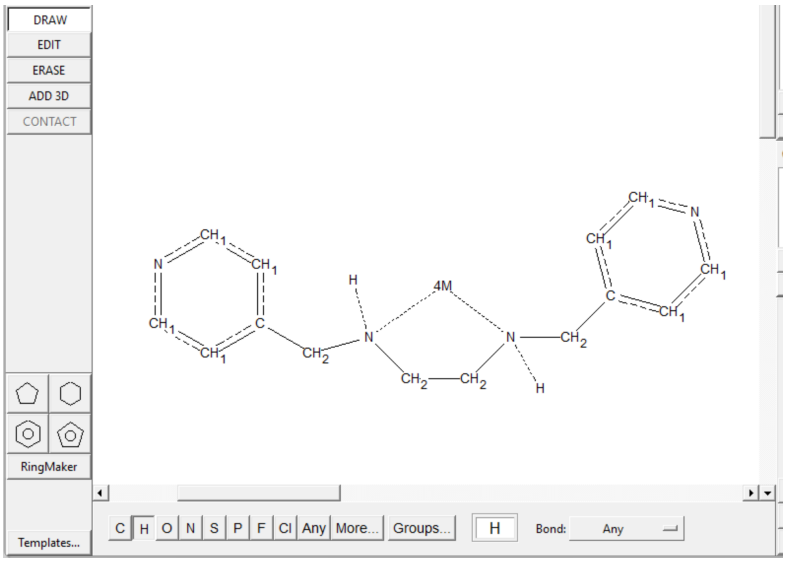

Fig. S3: Search query used to generate the hitlist of **enmepy** chelates in the CSD. 62 hits were found in the CSD version 5.45 (November 2023 with updates included until September 2024).

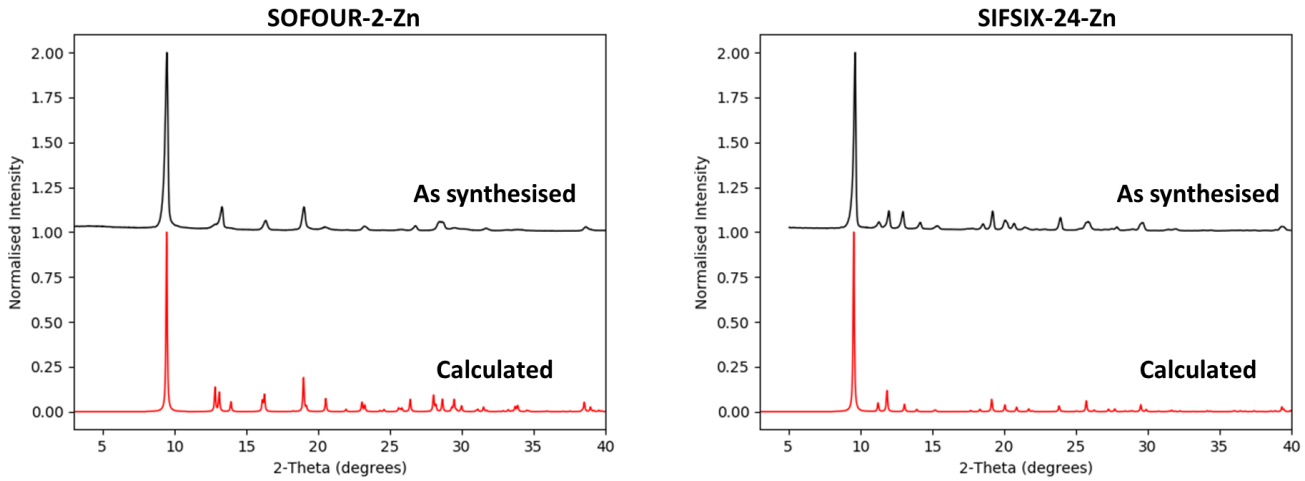

Fig. S4: PXRD patterns of as synthesised samples of **SOFOUR-2-Zn** and **SIFSIX-24-Zn** compared to their calculated PXRD patterns.

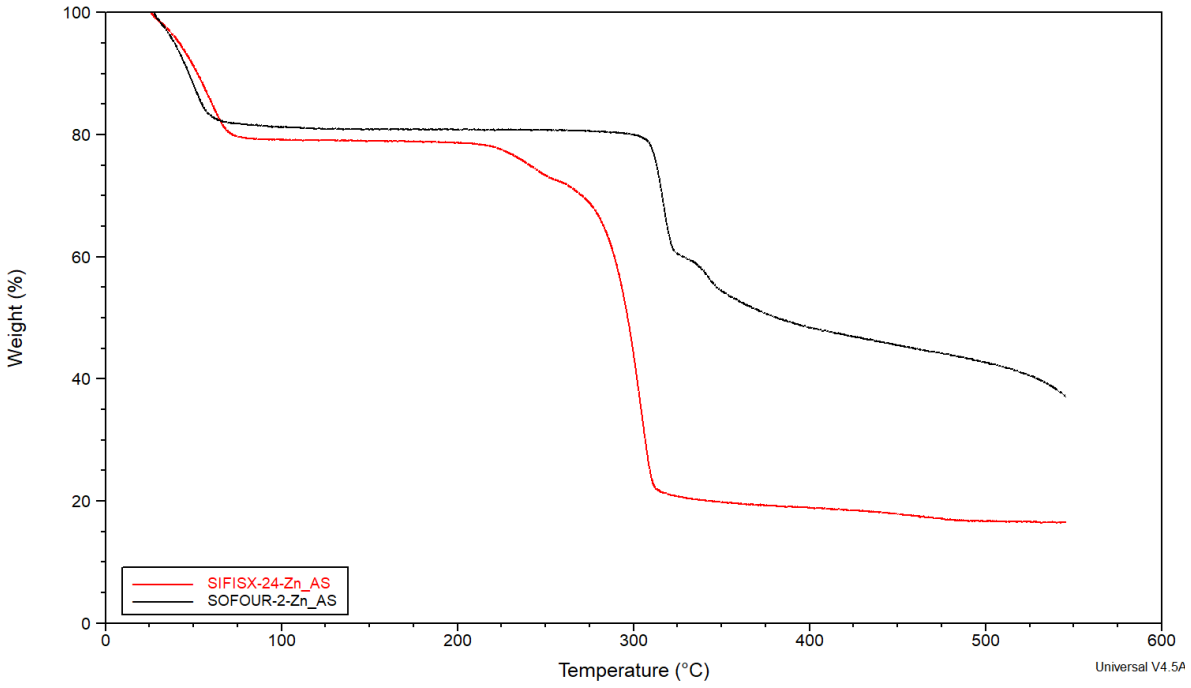

Fig. S5: TGA curves for **SOFOUR-2-Zn** and **SIFSIX-24-Zn**.

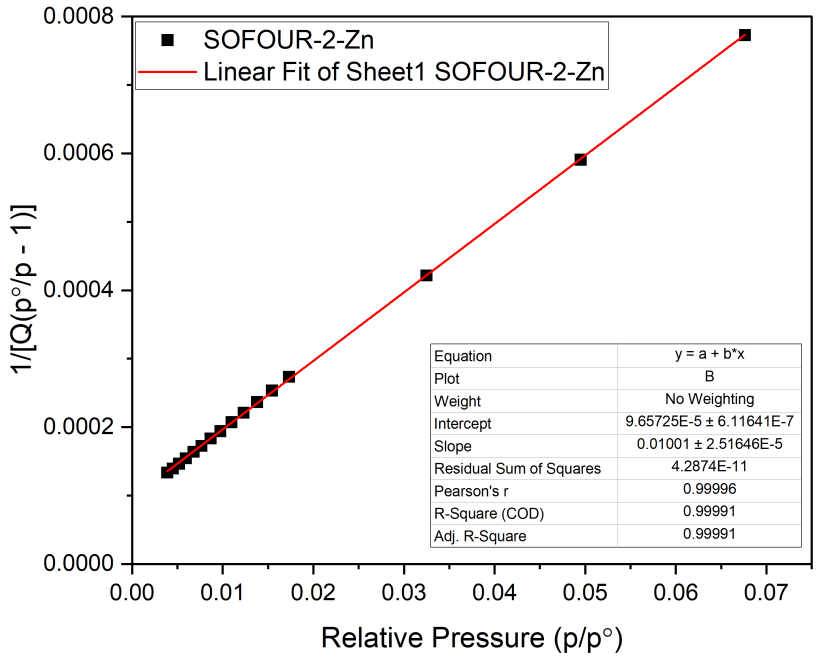

Fig. S6: BET plot for **SOFOUR-2-Zn** 195 K CO_2.

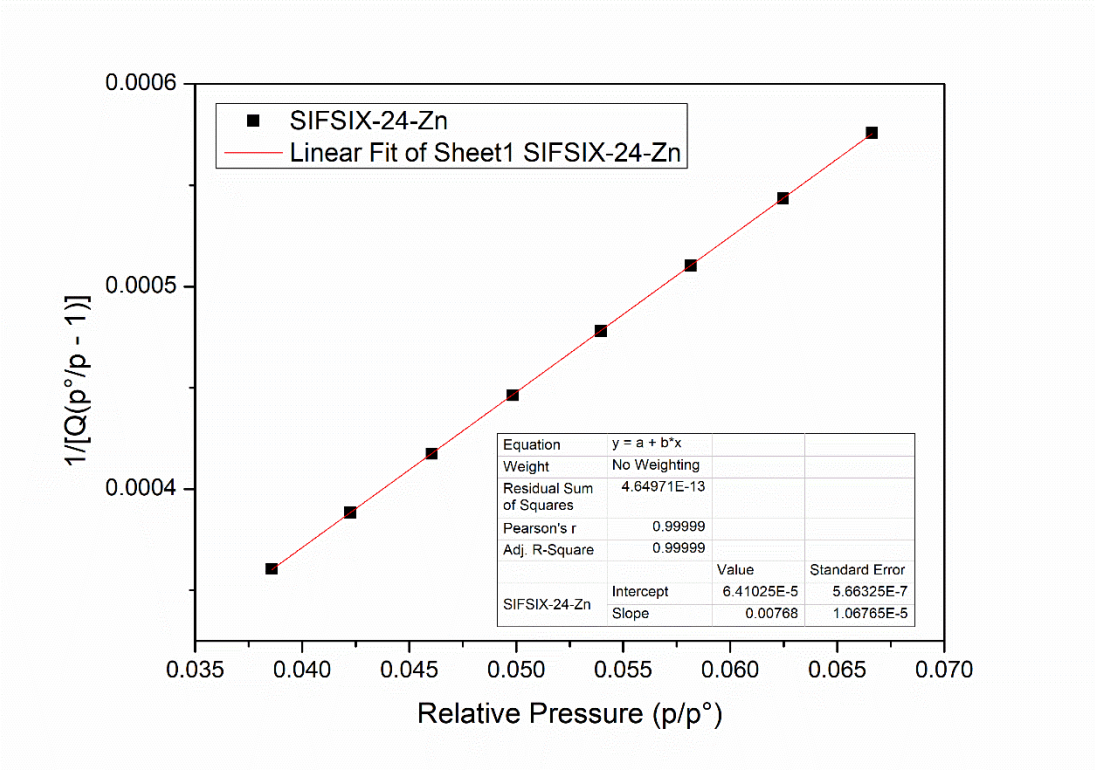

Fig. S7: BET plot for **SIFISIX-24-Zn** 195 K CO_2.

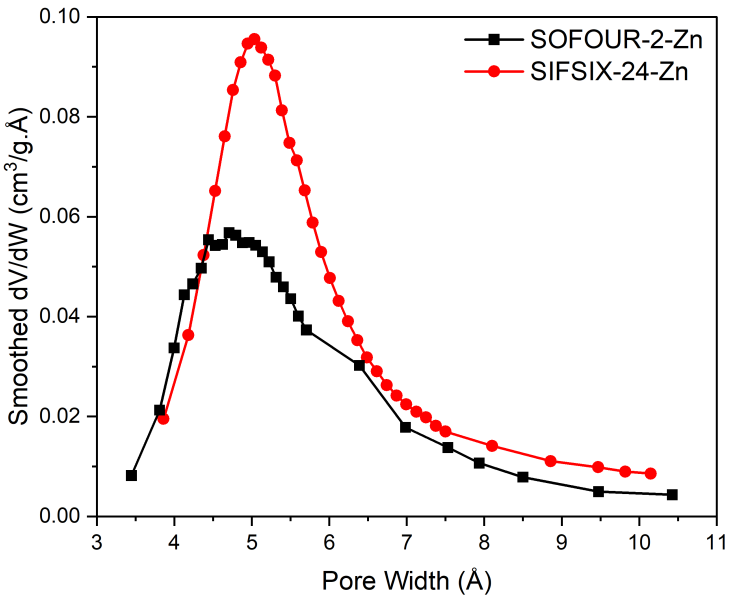

Fig. S8: The Horvath-Kawazoe differential pore volume plots for **SOFOUR-2-Zn** and **SIFSIX-24-Zn** from 195 K CO_2 isotherms.

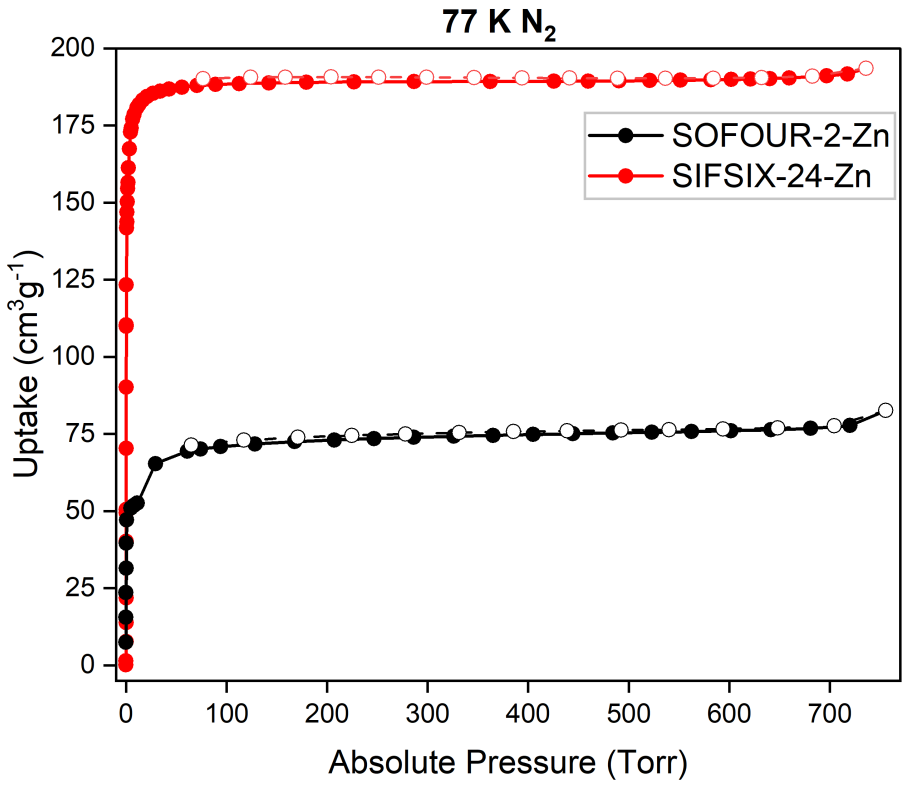

Fig. S9: 77 K N_2 sorption isotherms for **SOFOUR-2-Zn** and **SIFSIX-24-Zn**.

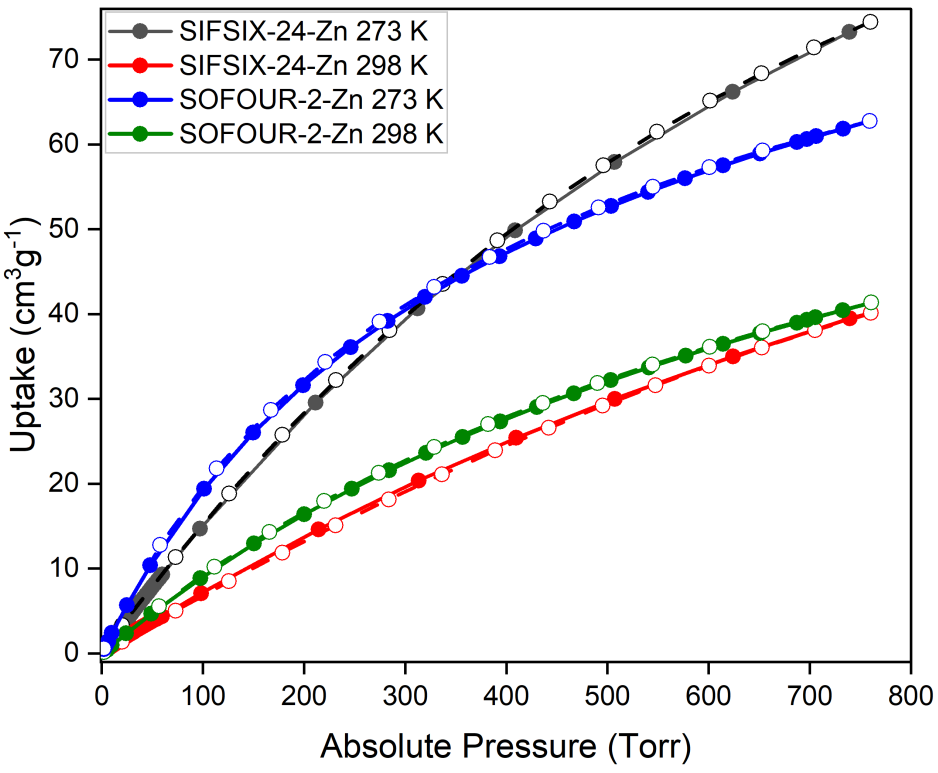

Fig. S10: 298 K and 273 K CO_2 sorption isotherms for **SIFSIX-24-Zn** and **SOFOUR-2-Zn**.

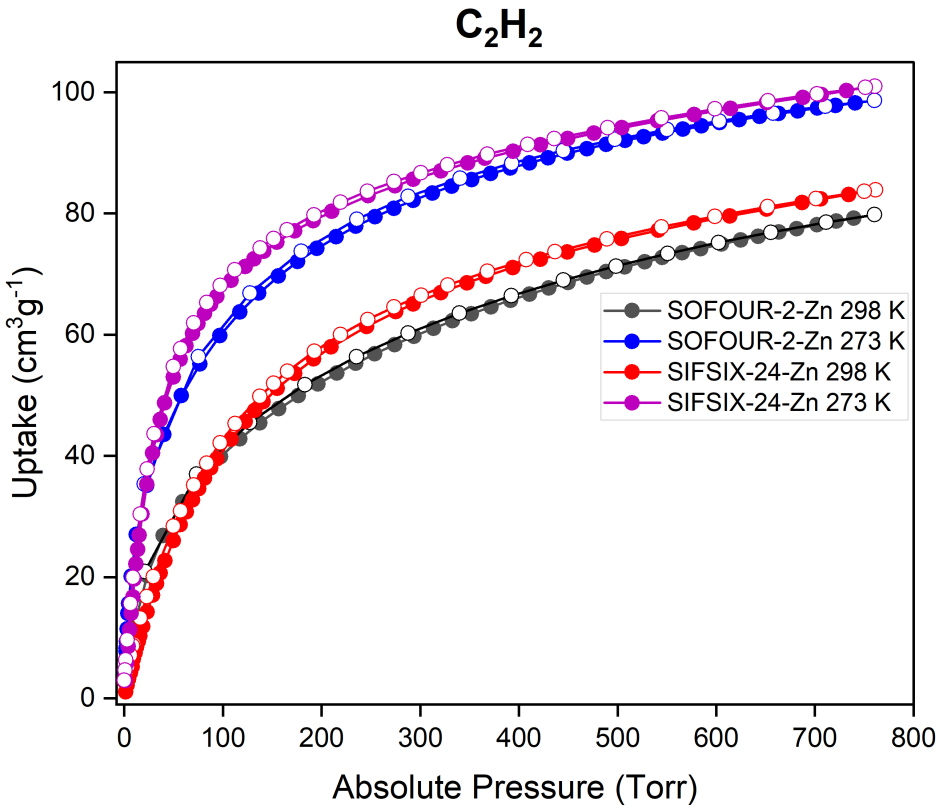

Fig. S11: 298 K and 273 K C_2H_2 sorption isotherms for **SOFOUR-2-Zn** and **SIFSIX-24-Zn**.

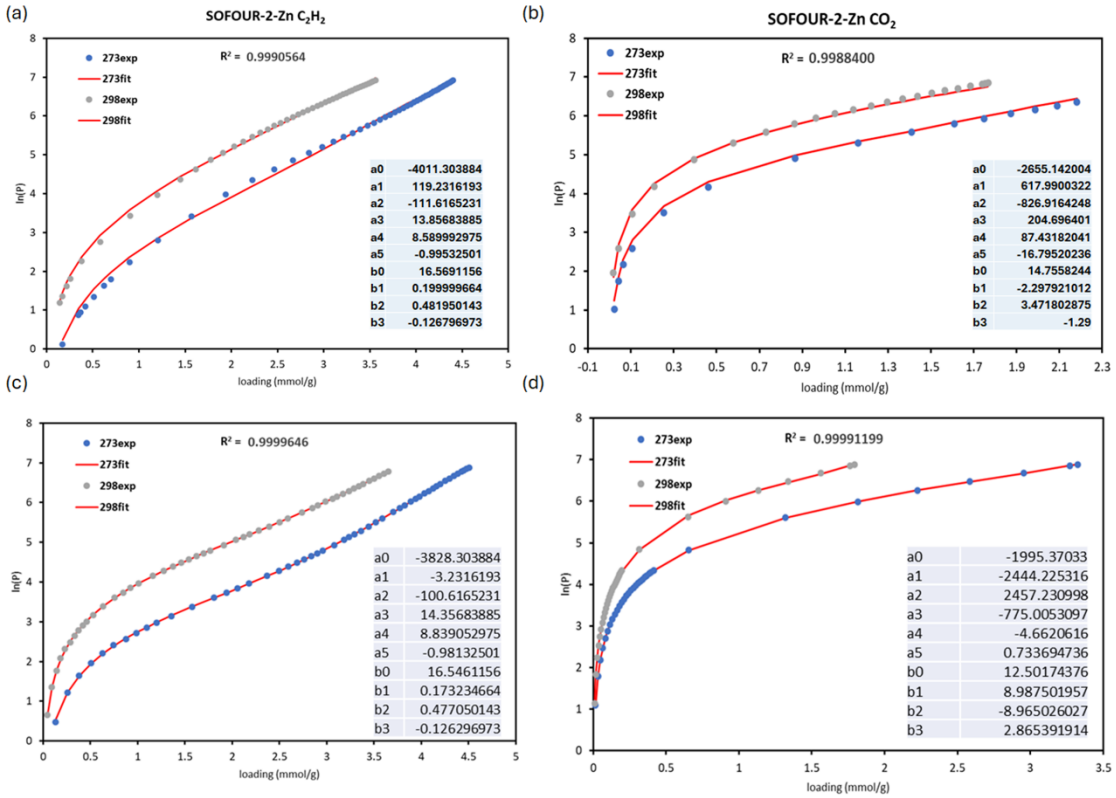

Fig. S12: Virial fits and parameters used for Q_{st} calculations for; a) **SOFOUR-2-Zn** C_2H_2 at 273 K and 298 K; b) **SOFOUR-2-Zn** CO_2 at 273 K and 298 K; c) **SIFSIX-24-Zn** C_2H_2 at 273 K and 298 K; d) **SIFSIX-24-Zn** CO_2 at 273 K and 298 K.

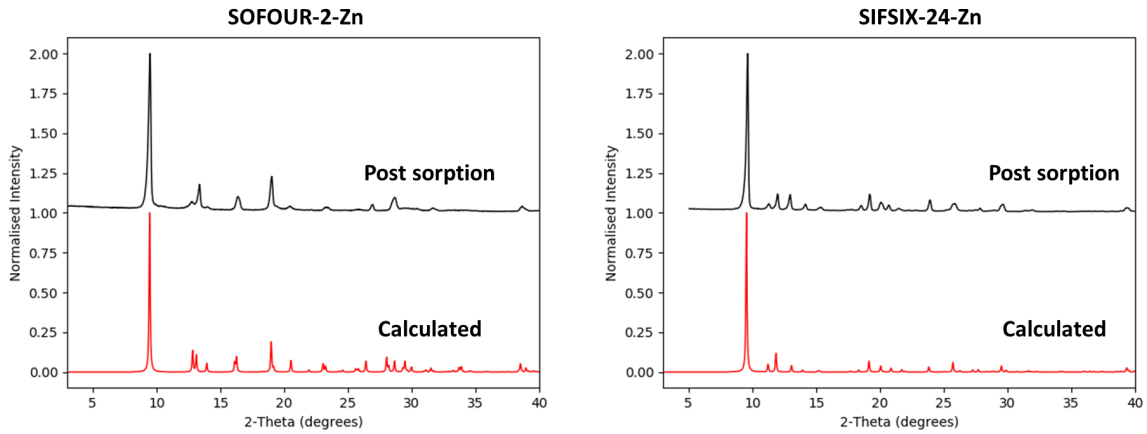

Fig. S13: PXRD patterns of samples of **SOFOUR-2-Zn** and **SIFSIX-24-Zn** after gas sorption compared to calculated PXRD patterns.

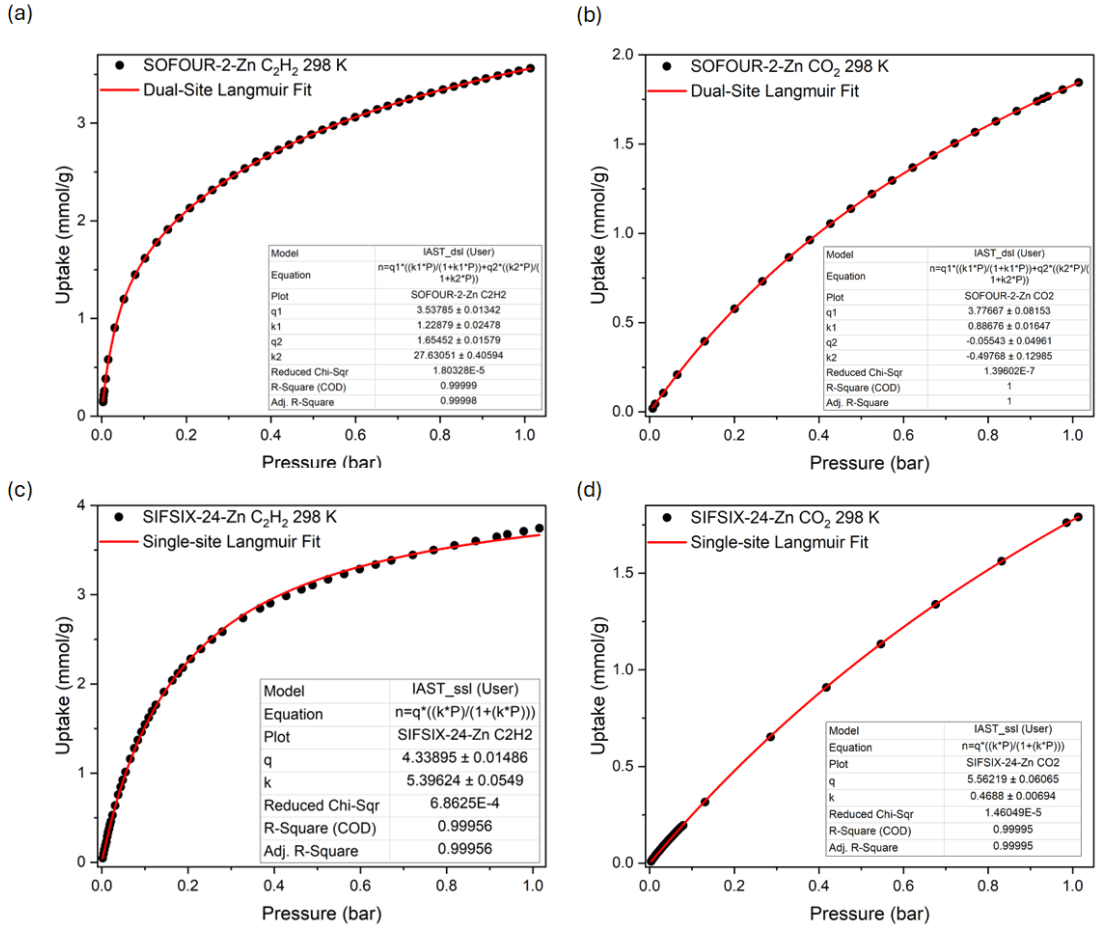

Fig. S14: a) Dual site Langmuir isotherm for 298 K C_2H_2 of **SOFOUR-2-Zn**; b) Dual site Langmuir isotherm for 298 K CO_2 of **SOFOUR-2-Zn**; c) Single-site Langmuir isotherm for 298 K C_2H_2 of **SIFSIX-24-Zn**; d) Single-site Langmuir isotherm for 298 K CO_2 of **SIFSIX-24-Zn**.

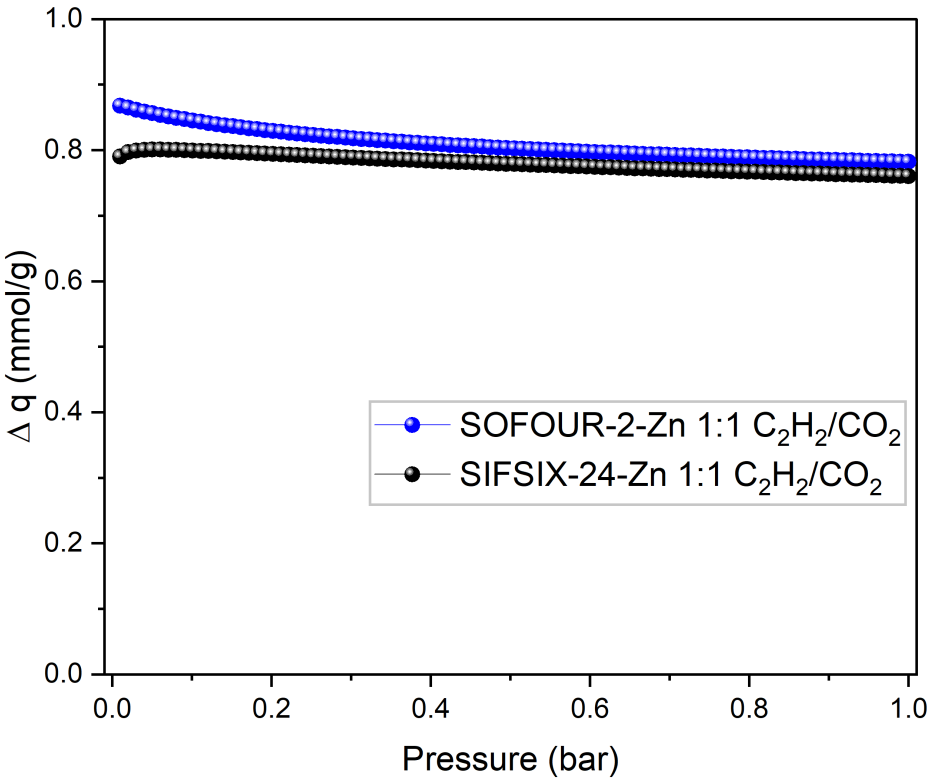

Fig. S15: IAST-based separation potential for C_2H_2/CO_2 (1/1, *v*/*v*) mixtures on **SOFOUR-2-Zn** and **SIFSIX-24-Zn**.

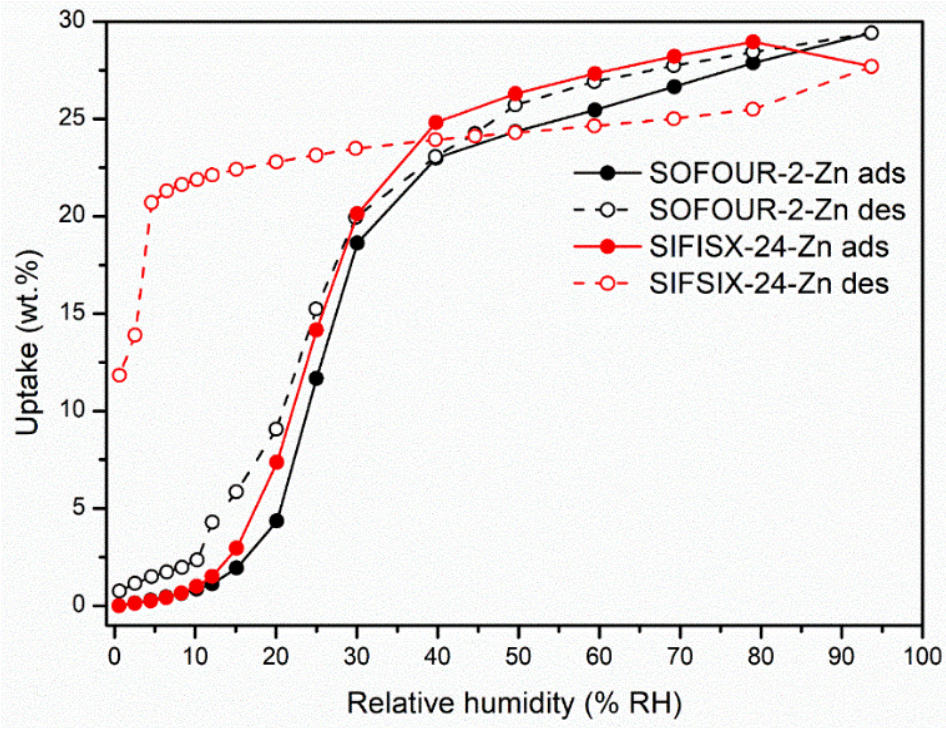

Fig. S16: Water vapour sorption isotherms for **SOFOUR-2-Zn** and **SIFSIX-24-Zn** at 27 °C measured using the DVS Adventure with air as carrier gas.

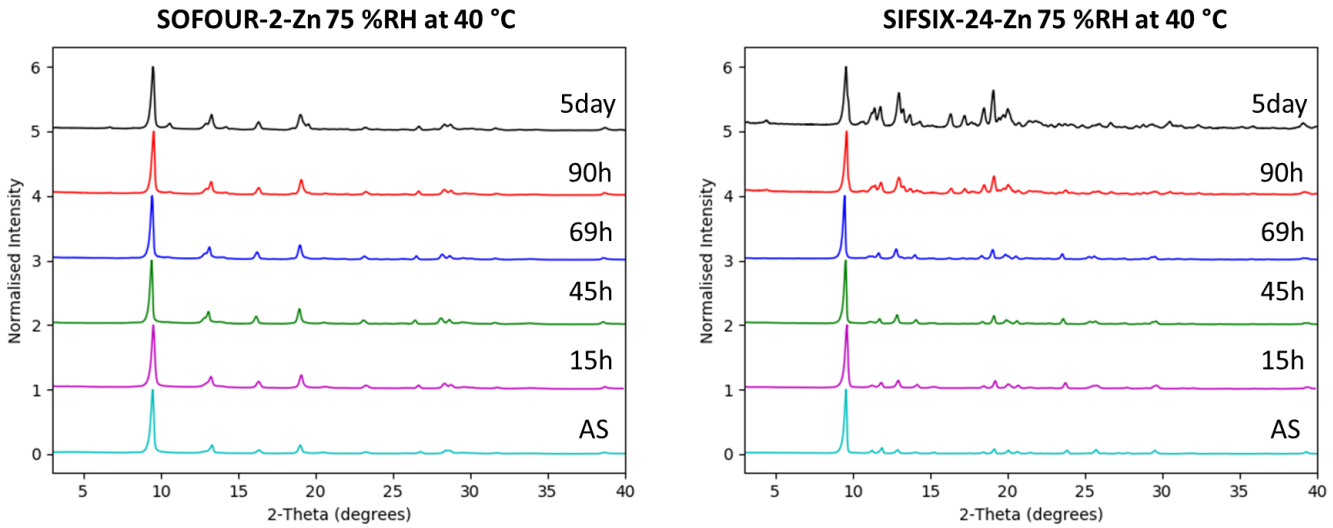

Fig. S17: Accelerated humidity stability testing (75 % RH, 40 °C) monitored by PXRD for **SOFOUR-2-Zn** and **SIFSIX-24-Zn**.

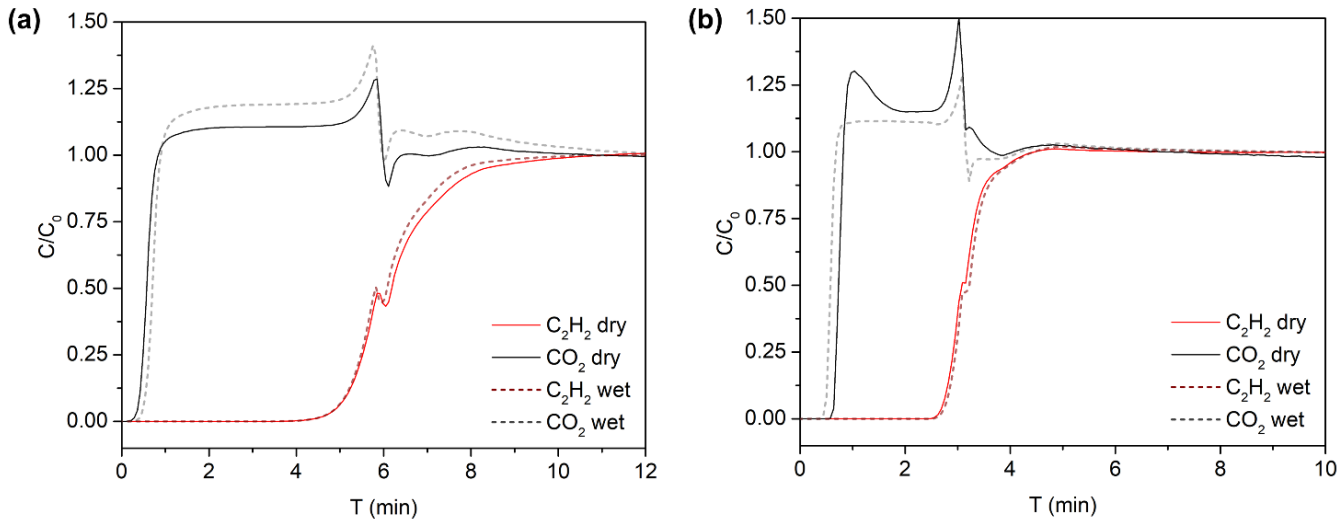

Fig. S18: Overlaid DCB plots of (a) **SOFOUR-2-Zn** and (b) **SIFSIX-24-Zn** for dry and wet gas streams of 1:2 C_2H_2:CO_2 (v/v) at a total flow rate of 15 cm^3 min^{-1}.

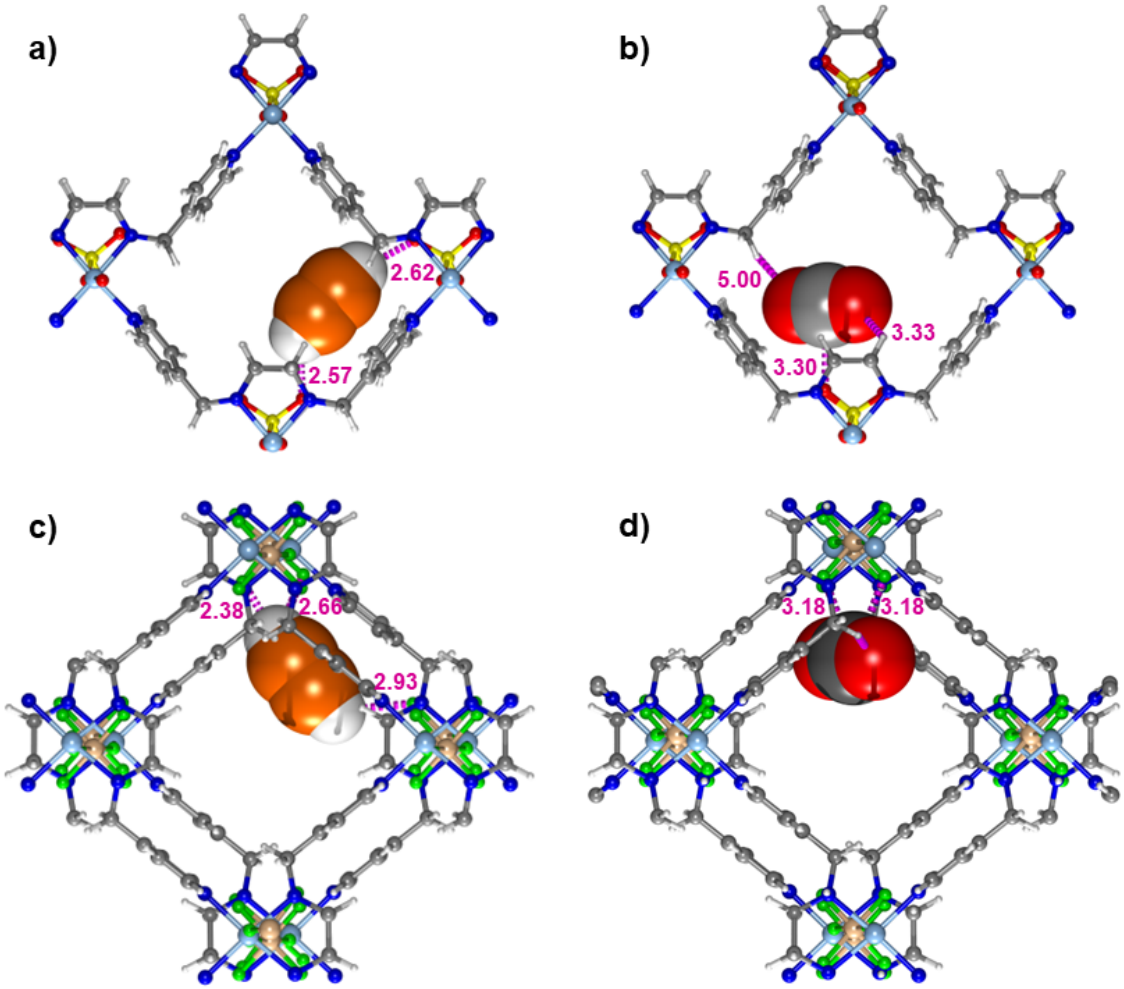

Fig. S19: The most plausible identified binding sites of (a) C_2H_2 and (b) CO_2 in **SOFOUR-2-Zn** and (c) C_2H_2 and (d) CO_2 in **SIFSIX-24-Zn** obtained by DFT calculations. (Colour codes: N = blue; Si = golden; S = yellow; F = green; Zn = lavender; O = red; H = white; C = grey and C(acetylene) = orange). The distances are highlighted using dashed magenta bonds and are given in Angstrom (Å), C_2H_2 and CO_2 molecules are shown in space-filling mode.

11. Supplementary Tables:

Table S1: Ethylene diamine chelates pillared by MF_6^{2-} anions (*vide* Fig. S2 for ligand numbers).

Refcode	Formula	Dimensionality	Potentially porous?	Ref
SINQOX	**$[Cu(L1)_2(TiF_6)]_n$**	1D	No	[9]
YAQLAF	**$[Cu(L1)_2(SiF_6)]_n$**	1D	No	[10]
YAQLAF01	**$[Cu(L1)_2(TiF_6)]_n$**	1D	No	[9]

Table S2: Ethylene diamine chelates pillared by SO_4^{2-} (vide Fig. S2 for ligand numbers).

Refcode	Formula	Network Dimensionality	Potentially porous?	Ref
AENCUS	**$[Cu(L1)(OH_2)_2(SO_4)]_n$**	1D	No	[11]
AENCUS01	**$[Cu(L1)(OH_2)_2(SO_4)]_n$**	1D	No	[12]
AENCUS02	**$[Cu(L1)(OH_2)_2(SO_4)]_n$**	1D	No	[13]
AENCUS03	**$[Cu(L1)(OH_2)_2(SO_4)]_n$**	1D	No	[14]
AENCUS04	**$[Cu(L1)(OD_2)_2(SO_4)]_n$**	1D	No	[14]
BIJMEP	**$[Zn(L2)_2(SO_4)]_n$**	1D	No	[15]
BIJMIT	**$[Cd(L2)_2(SO_4)]_n$**	1D	No	[15]
CIXZUG	**$[Cu(L6)(SO_4)]_n \cdot 2n(MeOH)$**	1D	Yes, guest solvent	[16]
DEHPUF	**$[Ni(L2)(SO4)]_n$**	1D	No	[17]
ETAZII	**$[Mn(L5)(SO_4)]_n \cdot n(ClO_4) \cdot n(H_2O)$**	1D	Yes, guest solvent	[18]
FOZZAX	**$[Cu(L5)(SO_4)]_n \cdot n(MeOH)$**	1D	Yes, guest solvent	[19]
FOZZEB	**$[Cu(L5)(SO_4)]_n \cdot 5n(H_2O)$**	1D	Yes, guest solvent	[19]
IYOBAC	**$[Fe(L2)_2(SO_4)]_n$**	1D	No	[20]
KOMNUY	**$[Co(L2)_2(SO_4)]_n$**	1D	No	[21]
MEWBUN	**$[Ni(L3)(OH_2)_2(SO_4)]_n \cdot n(H_2O)$**	1D	Yes, guest solvent	[22]
MEXRUF	**$[Cu(L8)(SO_4)]_n$**	1D	No	[23]
REPQIM	**$[Cu_2(L7)(SO_4)_2]_n$**	1D	No	[24]
RIGGEX	**$\{[Ni(L)(SO_4)]ClO_4.H_2O\}_n$**	1D	No	[25]
UGEWAG	**$[Cu_2(L4)(SO_4)_2]_n \cdot n(H_2O)$**	1D	Yes, guest solvent	[26]
VUYLOR	**$[Zn(L1)_2(SO_4)]_n$**	1D	No	[27]
VUYLOR01	**$[Zn(L1)_2(SO_4)]_n$**	1D	No	[28]
WOXWIS	**$[Cd(L12)(SO_4)]_n$**	3D	Yes, discrete voids	[29]
XAGNEZ	**$[Zn(L9)(SO_4)]_n \cdot ⅔n(H_2O)$**	1D	Yes, guest solvent	[30]
XEBTED	**$[Cd(L11)(SO_4)]_n \cdot 7/4n(H_2O)$**	1D tube	Yes, 1D pores	[31]
ZOMNOG	**$[Zn(enmepy)(SO_4)]_n \cdot 7n(H_2O)$**	3D	Yes, 1D pores	[32]

(nD = n-dimensional)

Table S3: Summary of **sql** nets formed by **enmepy** found in the CSD.

REFCODE	sql type	Stacking	Pillar	Ref
BOCYIF	Homochiral	Homochiral	None	[33]
DIFXAV	Homochiral	Homochiral	None	[34]
DIFXEZ	Homochiral	Racemic, layers alternate direction	None	
DIFXID	Homochiral	Homochiral	None	
DOLCIT	Racemic	N/A	None	[35]
DOLCOZ	Homochiral	Racemic, layers alternate direction	None	
DOLDOA	Homochiral	Homochiral	None	
HEBCEA	Homochiral	Homochiral	tsbdc	[36]
ILIFOA	Homochiral	Racemic, layers alternate direction	None	[37]
OKEQEC	Homochiral	Homochiral	None	[38]
OKEQIG	Homochiral	Homochiral	None	
OKEQOM	Homochiral	Racemic, mirror parallel to layers	None	
OKEQUS	Homochiral	Racemic, layers alternate direction	None	
OKERAZ	Homochiral	Racemic, layers alternate direction	None	
OKERIH	Racemic	N/A	None	
OKERON	Homochiral	Racemic, layers alternate direction	None	
OKERUT	Racemic	N/A	None	
OKESAA	Racemic	N/A	None	
QEBDIN	Homochiral	Racemic, layers alternate direction	1,4-bdc	[39]
QETBUP	Homochiral	Racemic, layers alternate direction	1,4-bdc	[40]
QETCAW	Homochiral	Racemic, layers alternate direction	1,4-bdc-NH_2	
RESYUL	Racemic	N/A	None	[41]
RESZAS	Homochiral	Racemic, layers alternate direction	None	
VIRWOK	Homochiral	Complex, 4 directions	None	[42]
VIRWUQ	Homochiral	Complex, 4 directions	None	
WOJGAH	Homochiral	Homochiral	L/D-NCG	[43]
ZOMNAS	Homochiral	Racemic, layers alternate direction	None	[32]
ZOMNEW	Homochiral	Homochiral	MoO_4^{2-}	
ZOMNIA	Homochiral	Homochiral	MoO_4^{2-}	
ZOMNOG	Homochiral	Homochiral	SO_4^{2-}	
ZOMNUM	Homochiral	Homochiral	CrO_4^{2-}	

L/D-NCG = L/D-*N*-carbamylglutamate

Table S4: Single-crystal X-ray data for **SIFSIX-24-Zn.**

Empirical formula	$C_{14}H_{18}F_6N_4SiZn$
CCDC entry	2206134
Formula weight	449.78
Temperature/K	100.00
Crystal system	orthorhombic
Space group	$C222_1$
a/Å	12.704(4)
b/Å	13.535(4)
c/Å	14.921(3)
α/°	90
β/°	90
γ/°	90
Volume/Å^3	2565.5(12)
Z	4
ρ_{calc}g/cm^3	1.165
μ/mm^{-1}	2.216
F(000)	912.0
Crystal size/mm^3	0.055 × 0.036 × 0.025
Radiation	CuKα (λ = 1.54184)
2θ range for data collection/°	9.548 to 118.084
Index ranges	-13 ≤ h ≤ 13, -14 ≤ k ≤ 13, -16 ≤ l ≤ 16
Reflections collected	6541
Independent reflections	1805 [R_{int} = 0.1245, R_{sigma} = 0.1074]
Data/restraints/parameters	1805/41/111
Goodness-of-fit on F^2	0.979
Final R indexes [I>=2σ (I)]	R_1 = 0.0709, wR_2 = 0.1692
Final R indexes [all data]	R_1 = 0.1088, wR_2 = 0.1914
Largest diff. peak/hole / e Å^{-3}	1.01/-0.66
Flack parameter	0.5(2)

Table S5: Comparison of sorption parameters for the leading C_2H_2 selective physisorbent materials that exhibit C_2H_2/CO_2 separation.

Adsorbent	Driving force	C_2H_2 uptake (mmol/g)	CO_2 uptake (mmol/g)	$Q_{st}(C_2H_2)$ (kJ/mol)	$Q_{st}(CO_2)$ (kJ/mol)	S_{AC} (1:1)	Ref.
SOFOUR-2-Zn	Electrostatics	2.6	1.4	34.3	21.9	8.1	This work
SIFSIX-24-Zn	Electrostatics	3.7	1.8	31.8	17.1	7.4	This work
SOFOUR-TEPE-Zn	Electrostatics	3.98	0.63	45.5	26.3	16833	65
SIFSIX-dps-Cu	Sieving	4.57	0.6[e]	60.5	NA	1787	66
UTSA-300a	Sieving	3.08	0.15	57.6	NA	743	67
GeFSIX-dps-Cu	Sieving	4.04	0.49[e]	56.3	NA	172	65
CPL-1-NH_2	Sieving	1.84	0.21	50	32.4	119	67
Cu@UiO-66-$(COOH)_2$	UMC	2.31	0.89	74.5	28.9	73	69
ZNU-1	Electrostatics	3.4	1.7	54.0	44.0	56.6	70
ATC-Cu	UMC	5.01	NA	79.1	NA	53.6	71
ZJU-74a	UMC	3.83	3.08	44.5	30	36.5	72
Zn_2(bpy)(btec)	Electrostatics	4.17	1.29	28.7	24.8	33.3	73
sql-16-Cu-NO3-α	Electrostatic	1.55	0.74	25.6	38.6	27.8	74
NKMOF-1-Ni	UMC	2.72	2.28	60.3	40.9	26	75
ZJU-196	Electrostatics	3.70	0.40	39.2	NA	25.0[c]	76
FeNi-M'MOF	UMC	4.29	2.72	27	24.5	24	77
$Ni_3(HCOO)_6$	Electrostatics	4.2	3.04	40.9	24.5	22	78
ZJU-280	Electrostatics	4.7	3.1	51.0	39.0	18.1	79
TCuCl	Electrostatics	3	2	41	30.1	16.9	80
BSF-3	Electrostatics	3.56	2.11	42.7	25.5	16.3	81
DICRO-4-Ni-i	Electrostatics	1.92	1.03	37.7	33.9	13.9	82
JCM-1	Electrostatics	3.35	1.7	36.9	33.4	13.7	83
SNNU-65-Cu-Sc	UMC	7.99	3.14	44.9	22.2	13.5	84
pacs-CoMOF-2a	UMC	5.40	2.81	34.2	24	13	85
Ni_2(L-asp)$_2$(bpy)	Electrostatics	2.68	1.40	16.6	24.2	12.6	86
MIL-100(Fe)	UMC	5.31[d]	2.50[d]	65	NA	12.5[d]	87
ZJU-40a	UMC	9.64	3.34	34.5	NA	11.5	88
[Co_2(HCOO)$_2$(CPT)$_2$]	Electrostatics	6.47	2.68	33	27	11	89
CAU-10-NH_2	Amine sites	4.3[f]	2.5[f]	31.3	24.5	10.8	90
SIFSIX-21-Cu	Electrostatics	3.9	1.5	36.3	24.0	10.0	91
TIFSIX-2-Cu-i	Electrostatics	4.1	4.3	46.3	34.2	10	92
ZJUT-2a [b]	Electrostatics	3.39	2.19	41.5	31.5	10	93
MIL-160	Electrostatics	9.5	4.0	31.8	26.9	10	94
SNNU-37(Fe)	UMC	4.9	2.1	34.4	33.4	9.9	95
BSF-4	Electrostatics	2.38	1.6	35	24.5	9.8	96
NbOFFIVE-3-Cu	Electrostatics	4.0	1.6	41.9	24.8	9.5	91
TCuBr	Electrostatics	2.8	2	36.8	26.8	9.5	80
NbOFFIVE-dps-Cu	Electrostatics	1.65	1.10	53.6	NA	9	66
UTSA-74a	UMC	4.78	3.17	31.7	25	9	97
CPL-1	Electrostatics	2.01	1.26	45.5	36.6	9	68

TIFSIX-4-Cu	Electrostatics	3.5	2.0	40.6	24.0	8.3	91
iMOF-6C	Electrostatics	1.2	0.68	38	N/A	8	98
SIFSIX-21-Ni	Electrostatics	4.0	1.3	37.9	19.8	7.8	91
TIFSIX-4-Ni	Electrostatics	3.8	2.0	41.4	27.4	7.6	91
$[Zn_3(HCOO)_6]_n$	Electrostatics	3.5	3.1	41.5	25.4	7.4	99
SNNU-150-Al	UMC	4.33	1.98	29	24	7.27	100
ZJU-60a [a]	UMC	6.7	3.3	17.6	15.2	6.7[a]	101
SNNU-65-Cu-Fe	UMC	7.25	2.9	28.2	21.8	6.7	84
SOFOUR-1-Zn	Electrostatics	3.1	3.6	57.0	33.0	6.6	102
NTU-55[a]	UMC	6.05	3.13	25	22	6.6[a]	103
SIFSIX-22-Zn	Electrostatics	5.7	4.2	36.5	25.0	6.5	102
UTSA-83	UMC	0.53	0.17	24.4	16.6	6.2	104
DZU-1	Electrostatics	4.0	3.0	3.17	30.6	6.1	105
TIFSIX-2-Ni-i	Electrostatics	4.21	4.54	40	34	6.1	106
NbOFFIVE-3-Ni	Electrostatics	3.8	1.9	36.7	25.0	6.0	91
PCP-33	UMC	5.44	2.62	27.5	26.2	6	107
NTU-66-Cu	UMC	4.98	2.19	32.3	21.7	6	108
MUF-17[d]	Electrostatics	3.01	2.51	49.5	33.8	6	109
iMOF-5C	Electrostatics	1.5	0.71	35.5	N/A	6	98
FJI-H8-Me	UMC	10.2	4.73	33.70	21.77	≈ 6	110
CPM-107op	Electrostatics	4.35	1.7	32	24	5.7	111
ZJNU-13	Electrostatics	5.29	3.92	33.5	22.5	5.64	112
SNFSIX-2-Zn	Electrostatics	5.0	3.9	41.3	43.3	5.6	113
IPM-101	Electrostatics	2.55	3.04	43.7	30.7	5.4	114
TCuI	Electrostatics	2.2	1.6	38.4	30.7	5.3	80
SIFSIX-Cu-TPA	Electrostatics	8.26	≈ 4.5	39.1	25.7	5.3	112
TIFSIX-6-Zn	Electrostatics	5.7	4.3	44.8	30.4	5.3	113
UTSA-98	UMC	3.7	1.8	22.8	18.3	5.2	115
UPC-110	Electrostatics	3.28	1.08	24.6	16	5.1	116
BSF-2	Electrostatics	1.85	1.33	37.3	28.7	5.1	80
JXNU-5a	UMC	2.5	1.55	32.9	25.2	5	117
GEFSIX-4-Zn	Electrostatics	5.4	4.4	44.8	≈ 34	5.0	113
ZRFSIX-3-Zn	Electrostatics	4.6	3.6	42.7	42.6	4.4	113
MFM-160a	Electrostatics	5.71	3.06	37	30	4	118

UMC = unsaturated metal centre; S_{AC} and uptake values at 298 K unless specified. [a] S_{AC} at 0.15 bar. [b]Uptake and S_{AC} at 296 K. [c]Uptake ratio at 298 K. [d]Uptake and S_{AC} at 293 K. [e]Uptake estimated from isotherm plot at 1 bar. [f]Volumetric uptake (mmol cm^{-3}).

Table S6. Uptakes and separation factors for **SOFOUR-2-Zn** and **SIFSIX-24-Zn** determined from DCB experiments.

Adsorbent	Sample mass (g)	Inlet C_2H_2 flow (cm^3 min^{-1})	Inlet CO_2 flow (cm^3 min^{-1})	C_2H_2 uptake (cm^3 g^{-1})	CO_2 uptake (cm^3 g^{-1})	α_{AC}	Min. effluent CO_2 purity
SOFOUR-2-Zn	**0.490**	0.50	0.50	47.04	23.24	2.05	99.989 %
SIFSIX-24-Zn	**0.375**	0.50	0.50	53.04	10.09	5.26	99.991 %

Table S7. Productivity and purity values for **SOFOUR-2-Zn** and **SIFSIX-24-Zn** determined from TPD experiments.

Adsorbent	Sample mass	He flow (cm^3 min^{-1})	> 98% C_2H_2 Interval (min g^{-1})	> 98% C_2H_2 Productivity (L kg^{-1} / mol kg^{-1})	> 99.5% C_2H_2 Interval (min g^{-1})	> 99.5% C_2H_2 Productivity (L kg^{-1} / mol kg^{-1})	Max. C_2H_2 purity
SOFOUR-2-Zn	**0.490 g**	20	4.2 -19.8	7.69 / 0.343	5.3-9.4	3.01 / 0.134	99.66 %
SIFSIX-24-Zn	**0.375 g**	20	5.02-26.96	9.45 / 0.422	5.8-23.9	8.75 / 0.391	99.92 %

Table S8. The adsorption enthalpy of C_2H_2 and CO_2 at their most plausible binding sites in **SOFOUR-2-Zn** and **SIFSIX-24-Zn** at room temperature obtained with DFT calculations compared with experimental data.

Sorbent	Sorbate	DFT ΔH_{ads} (kJ mol^{-1})	Experimental Q_{st} (kJ mol^{-1})
SIFSIX-24-Zn	C_2H_2	-38.9	-31.8
	CO_2	-32.1	-16.8
SOFOUR-2-Zn	C_2H_2	-41.2	-33.3
	CO_2	-30.9	-22.1

12. References:

1. B.-L. Fei, W.-Y. Sun, K.-B. Yu and W.-X. Tang, *J. Chem. Soc., Dalton Trans.*, 2000, DOI: 10.1039/A908910A, 805-811.
2. Bruker AXS Inc., 2021**, APEX4 v2021.4-0**.
3. G. M. Sheldrick, *SADABS: A PROGRAM FOR EXPLOITING THE REDUNDANCY OF AREA-DETECTOR X-RAY DATA*, University of Göttingen, Germany.
4. O. V. Dolomanov, L. J. Bourhis, R. J. Gildea, J. A. K. Howard and H. Puschmann, *J. Appl. Crystallogr.*, 2009, **42**, 339-341.
5. G. M. Sheldrick, *Acta Crystallogr. Sect. C: Cryst. Struct. Commun., 2015,* **71,** 3-8.
6. G. M. Sheldrick, *Acta Crystallogr. Sect. A: Found. Crystallogr.*, 2015, **71**, 3-8.
7. A. L. Spek, *Acta Crystallogr. Sect. C: Cryst. Struct. Commun.*, 2015, **71**, 9-18.
8. C. R. Groom, I. J. Bruno, M. P. Lightfoot and S. C. Ward, *Acta Crystallogr. Sect. B: Struct. Sci.*, 2016, **72**, 171-179.
9. J. Lhoste, K. Adil, A. Le Bail, M. Leblanc, A. Hemon-Ribaud and V. Maisonneuve, *J. Fluorine Chem.*, 2012, **134**, 29-34.
10. J. Hanikova, J. Cernak, J. Kuchar and E. Cizmar, *Inorg. Chim. Acta*, 2012, **385**, 178-184.
11. C. H. L. K. P. C. Healy, G. Smith, A. H. White, *Cryst. Struct. Commun.*, 1978, **7**, 556-570.
12. V. Manriquez, M. CamposVallette, N. Lara, N. GonzalezTejeda, O. Wittke, G. Diaz, S. Diez, R. Munoz and L. Kriskovic, *J. Chem. Crystallogr.*, 1996, **26**, 15-22.
13. M. K. Taylor, D. E. Stevenson, L. E. A. Berlouis, A. R. Kennedy and J. Reglinski, *J. Inorg. Biochem.*, 2006, **100**, 250-259.
14. O. V. Kravchina, A. I. Kaplienko, E. P. Nikolova, A. G. Anders, D. V. Ziolkovskii, A. Orendachova and M. Kajnakova, *Russ. J. Phys. Chem. B*, 2011, **5**, 209-214.
15. A. González Guillén, M. Oszajca, K. Luberda-Durnaś, M. Gryl, S. Bartkiewicz, A. Miniewicz and W. Lasocha, *Cryst. Growth Des.*, 2018, **18**, 5029-5037. L. G. Alves, M. Souto, F. Madeira, P. Adão, R. F. Munhá and A. M. Martins, *J. Organomet. Chem.*, 2014, **760**, 130-137.
16. L. G. Alves, M. Souto, F. Madeira, P. Adão, R. F. Munhá and A. M. Martins, *J. Organomet. Chem.*, 2014, **760**, 130-137.
17. A. B. González Guillén, P. Konieczny, K. Luberda-Durnaś, M. Oszajca, M. Kozieł, W. Łasocha, *New J. Chem*., 2022, **46**, 14786–14792.
18. S. Mossin, H. Weihe, H. Osholm Sørensen, N. Lima and R. Sessoli, *Dalton Trans.*, 2004, DOI: 10.1039/B314355D, 632-639.
19. I. Pérez-Toro, A. Domínguez-Martín, D. Choquesillo-Lazarte, E. Vílchez-Rodríguez, J. M. González-Pérez, A. Castiñeiras and J. Niclós-Gutiérrez, *J. Inorg. Biochem.*, 2015, **148**, 84-92.
20. A. González Guillén, M. Oszajca and W. Łasocha, *Polyhedron*, 2021, **206**, 115319.
21. P. Konieczny, A. B. Gonzalez-Guillén, K. Luberda-Durnaś, E. Čižmár, R. Pełka, M. Oszajca and W. Łasocha, *Dalton Trans.*, 2019, **48**, 7560-7570.
22. G. Schmidt and K. Merzweiler, *Acta Crystallogr. Sect. Sect. E: Struct. Rep. Online*, 2013, **69**, m197.
23. I. Carreira-Barral, I. Fernández-Pérez, M. Mato-Iglesias, A. De Blas, C. Platas-Iglesias and D. Esteban-Gómez, *Molecules*, 2018, **23**, 479.
24. D. A. Nation, A. E. Martell, R. I. Carroll and A. Clearfield, *Inorg. Chem.*, 1996, **35**, 7246-7252.
25. T. L. Morrison, I. Bhowmick and M. P. Shores, *Cryst. Growth Des.,* 2023, **23,** 3186–3194.
26. H. Lavrenyuk, O. Mykhalichko, B. Zarychta, V. Olijnyk and B. Mykhalichko, *J. Mol. Struct.*, 2015, **1095**, 34-41.
27. M. Lutz, S. Smeets and P. Parois, *Acta Crystallogr. Sect. Sect. E: Struct. Rep. Online*, 2010, **66**, M671-U713.
28. A. O. M. Kajňaková, M. Orendáč, A. Feher, M. Mal'arová, Z. Trávníček, *Acta Phys.Pol.,A*, 2008, **113**, 507.
29. L.-N. Zhu, Z.-P. Deng, L.-H. Huo and S. Gao, *CrystEngComm*, 2019, **21**, 7249-7259.
30. H. L. Zhu, J. L. Ma and D. Q. Wang, *Z. Anorg. Allg. Chem.*, 2004, **630**, 1317-1320.
31. M. A. Shipman, C. Price, A. E. Gibson, M. R. J. Elsegood, W. Clegg and A. Houlton, *Chem. Eur. J.*, 2000, **6**, 4371-4378.
32. Y. Wen, T. Sheng, Z. Sun, Z. Xue, Y. Wang, Y. Wang, S. Hu, X. Ma and X. Wu, *Chem. Commun.*, 2014, **50**, 8320-8323.
33. J. Huang, S. Zhou, S. Zhang, L. Wang, X.-T. Wu, Q.-L. Zhu and Y. Wen, *Sep. Purif. Technol.*, 2024, **336**, 126294.
34. Z. Liang, M. Huang, J. Huang, S. Zhang, Y. Wen, Q.-L. Zhu and X.-T. Wu, *Cryst. Growth Des.*, 2023, **23**, 3437–3446.
35. D.-D. Guo, L.-N. Zhu, X.-X. Meng, Z.-P. Deng, L.-H. Huo and S. Gao, *Appl. Organomet. Chem.*, 2019, **33**, e5056.
36. J. Tang, S. Zhou, M. Huang, Z. Liang, S. Su, Y. Wen, Q.-L. Zhu and X. Wu, *Inorg. Chem. Front.,* 2022, **9,** 3436–3443.
37. Y. Wen, T. Sheng, C. Zhuo, X. Zhu, S. Hu, W. Cao, H. Li, H. Zhang and X. Wu, *Inorg. Chem.*, 2016, **55**, 4199-4205.
38. Y. Wen, T. Sheng, X. Zhu, H. Zhang, C. Zhuo, S. Hu, W. Cao and X. Wu, *Eur. J. Chem.*, 2016, **22**, 5327-5334.

39. Y. Wen, T. Sheng, X. Zhu, C. Zhuo, S. Su, H. Li, S. Hu, Q.-L. Zhu and X. Wu, *Adv. Mater.*, 2017, **29**, 1700778.
40. S. Khatua, A. Santra, S. Padmakumar, K. Tomar and S. Konar, *ChemistrySelect*, 2018, **3**, 785-793.
41. Y. Wen, T. Sheng, S. Hu, Y. Wang, C. Tan, X. Ma, Z. Xue, Y. Wang and X. Wu, *CrystEngComm*, 2013, **15**, 2714-2721.
42. Y. Wen, T. Sheng, S. Hu, X. Ma, C. Tan, Y. Wang, Z. Sun, Z. Xue and X. Wu, *Chem. Commun.*, 2013, **49**, 10644-10646.
43. S. Zhang, J. Huang, L. Wang, H. Li, H. Dong, Q.-L. Zhu, Y. Wen and X.-T. Wu, *Adv. Opt. Mater.*, 2024, 12, 2400213.
44. A. Nuhnen and C. Janiak, *Dalton Trans.*, 2020, **49**, 10295-10307.
45. P. Atkins and J. de Paula, *Physical Chemistry*, Oxford University Press, Great Britain, 2010.
46. A. L. Myers and J. M. Prausnitz, *AlChE J.*, 1965, **11**, 121-127.
47. K. S. Walton and D. S. Sholl, AlChE J., 2015, 61, 2757-2762.
48. R. Krishna, *RSC Adv.*, 2017, **7**, 35724-35737.
49. R. Krishna, *ACS Omega*, 2020, **5**, 16987-17004.
50. C. M. Simon, B. Smit and M. Haranczyk, *Comput. Phys. Commun.*, 2016, **200**, 364-380.
51. N. S. Wilkins, A. Rajendran and S. Farooq, *Adsorption*, 2021, **27**, 397-422.
52. P. E. Blöchl, *Phys. Rev. B*, 1994, **50**, 17953-17979.
53. G. Kresse and J. Furthmüller, *Comput. Mater. Sci.* 1996, **6**, 15-50.
54. G. Kresse and J. Furthmüller, *Physical Review B*, 1996, **54**, 11169-11186.
55. J. Wellendorff, K. T. Lundgaard, A. Møgelhøj, V. Petzold, D. D. Landis, J. K. Nørskov, T. Bligaard and K. W. Jacobsen, *Phys. Rev. B*, 2012, **85**, 235149.
56. H. J. Monkhorst and J. D. Pack, *Phys. Rev. B*, 1976, **13**, 5188-5192.
57. A. Ghysels, T. Verstraelen, K. Hemelsoet, M. Waroquier and V. Van Speybroeck, *J. Chem. Inf. Model*, 2010, **50**, 1736-1750.
58. D. Dubbeldam, A. Torres-Knoop and K. S. Walton, *Mol. Simul.*, 2013, **39**, 1253-1292.
59. D. Dubbeldam, S. Calero, D. E. Ellis and R. Q. Snurr, *Mol. Simul.*, 2016, **42**, 81-101.
60. A. K. Rappe, C. J. Casewit, K. S. Colwell, W. A. Goddard and W. M. Skiff, *J. Am. Chem. Soc.*, 1992, **114**, 10024-10035.
61. C. E. Wilmer, K. C. Kim and R. Q. Snurr, *J. Phys. Chem. Lett.*, 2012, **3**, 2506-2511.
62. M. G. Martin and J. I. Siepmann, *J. Phys. Chem. B*, 1998, **102**, 2569-2577.
63. J. Pang, F. Jiang, M. Wu, C. Liu, K. Su, W. Lu, D. Yuan and M. Hong, *Nature Commun.*, 2015, **6**, 7575.
64. M. Fischer, F. Hoffmann and M. Fröba, *ChemPhysChem*, 2010, **11**, 2220-2229.
65. X. Liu, P. Zhang, H. Xiong, Y. Zhang, K. Wu, J. Liu, R. Krishna, J. Chen, S. Chen, Z. Zeng, S. Deng and J. Wang, *Adv. Mater.*, 2023, **35**, 2210415.
66. J. Wang, Y. Zhang, Y. Su, X. Liu, P. Zhang, R.-B. Lin, S. Chen, Q. Deng, Z. Zeng, S. Deng and B. Chen, *Nat. Commun.*, 2022, **13**, 200.
67. R.-B. Lin, L. Li, H. Wu, H. Arman, B. Li, R.-G. Lin, W. Zhou and B. Chen, *J. Am. Chem. Soc.*, 2017, **139**, 8022-8028.
68. L. Yang, L. Yan, Y. Wang, Z. Liu, J. He, Q. Fu, D. Liu, X. Gu, P. Dai, L. Li and X. Zhao, *Angew. Chem. Int. Ed.*, 2021, **60**, 4570-4574.
69. L. Zhang, K. Jiang, L. Yang, L. Li, E. Hu, L. Yang, K. Shao, H. Xing, Y. Cui, Y. Yang, B. Li, B. Chen and G. Qian, *Angew. Chem. Int. Ed.*, 2021, **60**, 15995-16002.
70. L. Wang, W. Sun, Y. Zhang, N. Xu, R. Krishna, J. Hu, Y. Jiang, Y. He and H. Xing, *Angew. Chem. Int. Ed.*, 2021, **60**, 22865-22870.
71. Z. Niu, X. Cui, T. Pham, G. Verma, P. C. Lan, C. Shan, H. Xing, K. A. Forrest, S. Suepaul, B. Space, A. Nafady, A. M. Al-Enizi and S. Ma, *Angew. Chem. Int. Ed.*, 2021, **60**, 5283-5288.
72. J. Pei, K. Shao, J.-X. Wang, H.-M. Wen, Y. Yang, Y. Cui, R. Krishna, B. Li and G. Qian, *Adv. Mater.*, 2020, **32**, 1908275.
73. Y. Chen, Y. Du, Y. Wang, R. Krishna, L. Li, J. Yang, J. Li and B. Mu, *AlChE J.*, 2021, **67**, e17152.
74. N. Kumar, S. Mukherjee, A. A. Bezrukov, M. Vandichel, M. Shivanna, D. Sensharma, A. Bajpai, V. Gascón, K.-i. Otake, S. Kitagawa and M. J. Zaworotko, *SmartMat*, 2020, **1**, e1008.
75. Y.-L. Peng, T. Pham, P. Li, T. Wang, Y. Chen, K.-J. Chen, K. A. Forrest, B. Space, P. Cheng, M. J. Zaworotko and Z. Zhang, *Angew. Chem. Int. Ed.*, 2018, **57**, 10971-10975.
76. L. Zhang, K. Jiang, L. Li, Y.-P. Xia, T.-L. Hu, Y. Yang, Y. Cui, B. Li, B. Chen and G. Qian, *Chem. Commun.*, 2018, **54**, 4846-4849.
77. J. Gao, X. Qian, R.-B. Lin, R. Krishna, H. Wu, W. Zhou and B. Chen, *Angew. Chem. Int. Ed.*, 2020, **59**, 4396-4400.
78. L. Zhang, K. Jiang, J. Zhang, J. Pei, K. Shao, Y. Cui, Y. Yang, B. Li, B. Chen and G. Qian, *ACS Sustain. Chem. Eng.*, 2019, **7**, 1667-1672.
79. Q.-L. Qian, X.-W. Gu, J. Pei, H.-M. Wen, H. Wu, W. Zhou, B. Li and G. Qian, *J. Mater. Chem. A.*, 2021, **9**, 9248-9255.
80. S. Mukherjee, Y. He, D. Franz, S.-Q. Wang, W.-R. Xian, A. A. Bezrukov, B. Space, Z. Xu, J. He and M. J. Zaworotko, *Eur. J. Chem.*, 2020, **26**, 4923-4929.

81. Y. Zhang, J. Hu, R. Krishna, L. Wang, L. Yang, X. Cui, S. Duttwyler and H. Xing, *Angew. Chem. Int. Ed.*, 2020, **59**, 17664-17669.
82. H. S. Scott, M. Shivanna, A. Bajpai, D. G. Madden, K.-J. Chen, T. Pham, K. A. Forrest, A. Hogan, B. Space, J. J. Perry Iv and M. J. Zaworotko, *ACS Appl. Mater. Interfaces*, 2017, **9**, 33395-33400.
83. J. Lee, C. Y. Chuah, J. Kim, Y. Kim, N. Ko, Y. Seo, K. Kim, T. H. Bae and E. Lee, *Angew. Chem. Int. Ed.*, 2018, **57**, 7869-7873.
84. J.-W. Zhang, M.-C. Hu, S.-N. Li, Y.-C. Jiang, P. Qu and Q.-G. Zhai, *Chem. Commun.*, 2018, **54**, 2012-2015.
85. D.-M. Chen, C.-X. Sun, N.-N. Zhang, H.-H. Si, C.-S. Liu and M. Du, *Inorg. Chem.*, 2018, **57**, 2883-2889.
86. W. Gong, H. Cui, Y. Xie, Y. Li, X. Tang, Y. Liu, Y. Cui and B. Chen, *J. Am. Chem. Soc.*, 2021, **143**, 14869-14876.
87. J. W. Yoon, J. S. Lee, S. Lee, K. H. Cho, Y. K. Hwang, M. Daturi, C.-H. Jun, R. Krishna and J.-S. Chang, *Eur. J. Chem.*, 2015, **21**, 18431-18438.
88. H.-M. Wen, H. Wang, B. Li, Y. Cui, H. Wang, G. Qian and B. Chen, *Inorg. Chem.*, 2016, **55**, 7214-7218.
89. D.-M. Chen, X.-H. Liu, J.-Y. Tian, J.-H. Zhang, C.-S. Liu and M. Du, *Inorg. Chem.*, 2017, **56**, 14767-14770.
90. X. Zhang, R.-B. Lin, H. Wu, Y. Huang, Y. Ye, J. Duan, W. Zhou, J.-R. Li and B. Chen, *Chem. Eng. J.*, 2022, **431**, 134184.
91. N. Kumar, S. Mukherjee, N. C. Harvey-Reid, A. A. Bezrukov, K. Tan, V. Martins, M. Vandichel, T. Pham, L. M. van Wyk, K. Oyekan, A. Kumar, K. A. Forrest, K. M. Patil, L. J. Barbour, B. Space, Y. Huang, P. E. Kruger and M. J. Zaworotko, *Chem*, 2021, **7**, 3085-3098.
92. K.-J. Chen, Hayley S. Scott, David G. Madden, T. Pham, A. Kumar, A. Bajpai, M. Lusi, Katherine A. Forrest, B. Space, John J. Perry and Michael J. Zaworotko, *Chem*, 2016, **1**, 753-765.
93. H.-M. Wen, C. Liao, L. Li, L. Yang, J. Wang, L. Huang, B. Li, B. Chen and J. Hu, *Chem. Commun.*, 2019, **55**, 11354-11357.
94. Y. Ye, S. Xian, H. Cui, K. Tan, L. Gong, B. Liang, T. Pham, H. Pandey, R. Krishna, P. C. Lan, K. A. Forrest, B. Space, T. Thonhauser, J. Li and S. Ma, *J. Am. Chem. Soc.*, 2022, **144**, 1681-1689.
95. S.-C. Fan, Y.-T. Li, Y. Wang, J.-W. Wang, Y.-Y. Xue, H.-P. Li, S.-N. Li and Q.-G. Zhai, *Inorg. Chem.*, 2021, **60**, 18473-18482.
96. Y. Zhang, L. Wang, J. Hu, S. Duttwyler, X. Cui and H. Xing, *CrystEngComm*, 2020, **22**, 2649-2655.
97. F. Luo, C. Yan, L. Dang, R. Krishna, W. Zhou, H. Wu, X. Dong, Y. Han, T.-L. Hu, M. O'Keeffe, L. Wang, M. Luo, R.-B. Lin and B. Chen, *J. Am. Chem. Soc.*, 2016, **138**, 5678-5684.
98. S. Dutta, S. Mukherjee, O. T. Qazvini, A. K. Gupta, S. Sharma, D. Mahato, R. Babarao and S. K. Ghosh, *Angew. Chem. Int. Ed.*, 2022, **61**, e202114132.
99. J.-H. Li, Y. Xie, M.-Y. Zhou, R.-B. Lin and X.-M. Chen, *Chem. Res. Chin. Univ.*, 2022, **38**, 87-91.
100. H.-J. Lv, Y.-P. Li, Y.-Y. Xue, Y.-C. Jiang, S.-N. Li, M.-C. Hu and Q.-G. Zhai, *Inorg. Chem.*, 2020, **59**, 4825-4834.
101. X. Duan, Q. Zhang, J. Cai, Y. Yang, Y. Cui, Y. He, C. Wu, R. Krishna, B. Chen and G. Qian, *J. Mater. Chem. A.*, 2014, **2**, 2628-2633.
102. D. Sensharma, D. J. O'Hearn, A. Koochaki, A. A. Bezrukov, N. Kumar, B. H. Wilson, M. Vandichel and M. J. Zaworotko, *Angew. Chem. Int. Ed.*, 2022, **61**, e202116145.
103. Q. Dong, Y. Guo, H. Cao, S. Wang, R. Matsuda and J. Duan, *ACS Applied Materials & Interfaces*, 2020, **12**, 3764-3772.
104. H. Cui, S. Chen, H. Arman, Y. Ye, A. Alsalme, R.-B. Lin and B. Chen, *Inorg. Chim. Acta*, 2019, **495**, 118938.
105. B.-Y. Zhu, T. Zhang, C.-H. Li, J.-W. Cao, Z.-Q. Zhang, W. Qi, G.-Y. Wang, Z.-H. Rong, Y. Wang and K.-J. Chen, *Inorg. Chem.*, 2022, **61**, 4555-4560.
106. M. Jiang, X. Cui, L. Yang, Q. Yang, Z. Zhang, Y. Yang and H. Xing, *Chem. Eng. J.*, 2018, **352**, 803-810.
107. J. Duan, W. Jin and R. Krishna, *Inorg. Chem.*, 2015, **54**, 4279-4284.
108. S. Chen, N. Behera, C. Yang, Q. Dong, B. Zheng, Y. Li, Q. Tang, Z. Wang, Y. Wang and J. Duan, *Nano Res.*, 2021, **14**, 546-553.
109. O. T. Qazvini, R. Babarao and S. G. Telfer, *Chem. Mater.*, 2019, **31**, 4919-4926.
110. Z. Di, C. Liu, J. Pang, C. Chen, F. Hu, D. Yuan, M. Wu and M. Hong, *Angew. Chem. Int. Ed.*, 2021, **60**, 10828-10832.
111. H. Yang, T. X. Trieu, X. Zhao, Y. Wang, Y. Wang, P. Feng and X. Bu, *Angew. Chem. Int. Ed.*, 2019, **58**, 11757-11762.
112. H. Li, C. Liu, C. Chen, Z. Di, D. Yuan, J. Pang, W. Wei, M. Wu and M. Hong, *Angew. Chem. Int. Ed.*, 2021, **60**, 7547-7552.
113. D. Sensharma, B. H. Wilson, N. Kumar, D. J. O'Hearn and M. J. Zaworotko, *Cryt. Growth Des.*, 2022, **22**, 5472-5480.
114. S. Sharma, S. Mukherjee, A. V. Desai, M. Vandichel, G. K. Dam, A. Jadhav, G. Kociok-Köhn, M. J. Zaworotko and S. K. Ghosh, *Chem. Mater.*, 2021, **33**, 5800-5808.
115. X. Wang, B. Wang, X. Zhang, Y. Xie, H. Arman and B. Chen, *Inorg. Chem.*, 2021, **60**, 18816-18821.

116. W. Fan, X. Wang, X. Liu, B. Xu, X. Zhang, W. Wang, X. Wang, Y. Wang, F. Dai, D. Yuan and D. Sun, *ACS Sustain. Chem. Eng.*, 2019, **7**, 2134-2140.
117. R. Liu, Q.-Y. Liu, R. Krishna, W. Wang, C.-T. He and Y.-L. Wang, *Inorg. Chem.*, 2019, **58**, 5089-5095.
118. W. J. F. Trenholme, D. I. Kolokolov, M. Bound, S. P. Argent, J. A. Gould, J. Li, S. A. Barnett, A. J. Blake, A. G. Stepanov, E. Besley, T. L. Easun, S. Yang and M. Schröder, *J. Am. Chem. Soc.*, 2021, **143**, 3348-3358.